The effect of shear-thickening on the stability of slot-die coating

Sunilkumar Khandavalli[a], Jonathan P. Rothstein[*,a]

[a]*Mechanical and Industrial Engineering, University of Massachusetts Amherst, MA 01003 USA*

Abstract

Slot die coating is an economical roll-to-roll processing technique with potential to revolutionize the fabrication of nano-patterned thin films at high throughput. In the present study, we have investigated the impact of shear-thickening of the coating fluid on the stability of slot die coating. For the coating fluid, we chose as a model system fumed silica nanoparticles dispersed in polypropylene glycol. These dispersions exhibit shear and extensional thickening characterized through steady shear and capillary break-up measurements. The critical web velocity for the onset of coating defect for different flow-rates was measured, while the type of coating defect was visualized using a high speed camera. For the shear thickening particle dispersions, the coating failed through the onset of a ribbing instability. The critical web velocity for the onset of coating defect was found to decrease with increasing particle concentration and increasing fluid viscosity. The minimum wet thickness was studied as a function of capillary number for the particle dispersions and compared with a series of Newtonian fluids with similar viscosities. In all cases, shear-thickening behavior was found to stabilize coating by reducing the minimum wet coating thickness when compared against a Newtonian fluid with similar viscosity at the same capillary number. Conversely, the shear-thinning fluids tested destabilized the coating by increasing the minimum wet thickness when compared against a Newtonian at the same capillary number. The impact of shear-thickening on slot-die coating was further studied by quantifying the evolution of the ribbing instability with increasing web speed and by conducting tests over a wide range of coating gaps.

Keywords: Slot die, Coating, Shear thickening, Colloids, Extensional rheology, Operating window, Ribbing

[*]Corresponding author at: Mechanical and Industrial Engineering, University of Massachusetts Amherst, MA 01003 USA, Tel.:+1 413 577 0110; fax: +1 413 545 1027

Email address: `rothstein@ecs.umass.edu` (Jonathan P. Rothstein[*,])

Introduction

Roll to roll printing is a continuous high-throughput, low-cost and large area technology which is utilized in a number of industrial and commercial processes for fabricating flexible films. Compared to conventional fabricating methods, roll to roll technology has the potential to significantly lower the cost of manufacturing of flexible devices. Slot-die coating is a roll-to-roll processing technology used to efficiently obtain coating with excellent uniformity[1]. It is commonly used in many applications such as adhesive and magnetic tapes, imaging films[2], solar cells[3], OLEDs[4], and lithium-ion battery electrodes[5]. Slot-die coating is a pre-metered coating method where the desired thickness is predetermined by setting the operating parameters, feed flow rate and substrate velocity. In slot-die coating process, the coating fluid is pumped through a narrow slit of the die, where it is distributed uniformly and coated onto the moving substrate under the die. A stable and uniform coating is obtained only for a certain range of operating parameters, flow rates and substrate velocities. This stable region is known as the operating window[6]. Outside this window, several coating defects can be observed such as air entrainment, flooding, ribbing, dripping and streaklines[7,8]. In many applications, a wider operating window is desired to delay the onset of the coating defects for faster web speeds and high throughputs.

Numerous investigations, experimental, theoretical and numerical computations[2,6,9–14] have been dedicated to investigating the factors affecting the operating window and the mechanism of evolution of coating defects[15–17]. Ruschak[6] examined the role of capillary pressures on the coating bead stability through quasi-static lubrication theory. Higgins and Scriven[12] extended the study to include viscous effects. Lee *et. al.*[11] and Gutoff and Kendrick[9] experimentally determined the limiting operating parameters for stable coating, termed as low-flow limit, or minimum wet thickness. It is defined as the maximum coating speed for a given flow-rate (film thickness) or minimum flow-rate for a given coating speed at which a uniform coating is possible[13]. The variation of minimum wet thickness or low-flow limit is commonly studied as a function of capillary number, *Ca*. The capillary number is the ratio of viscous to capillary forces given by $Ca = \eta V/\sigma$. Where η is fluid viscosity, V is the substrate velocity and σ is the fluid surface tension. For Newtonian solutions, three regimes of minimum wet thickness versus capillary number have been observed[10,11,13,18]. At low capillary number regime, the minimum wet thickness was found to increase with capillary number. At moderate capillary number, the minimum wet thickness was found to be independent of capillary number.

At large capillary number, the minimum wet thickness was found to decrease with increasing capillary number. Using flow visualization techniques, the mechanisms of the instability of the coating bead at upstream and downstream have also been studied[2,8,10,13,19]. The shape of the fluid meniscus between die lip and the substrate at the low-flow limit has been correlated to different types of coating defects. The operating window can also be expanded by applying a vaccum upstream to create a pressure gradient across the coating bead and reduce the likelihood of air entrainment[1,2,14,20].

In printing and coatings, the coating fluids are commonly non-Newtonian or viscoelastic due to the addition of polymer additives or particles to the coating fluids. There have been several studies through experiments, flow visualization techniques[2,7,18,21] and numerical simulations[14–16,21,22] investigating the effect of polymer additives on the operating window of slot-die coating. Ning $et.$ $al.$[7] had examined the effect of polymer concentration on the maximum coating speed for a stable coating. An optimal polymer concentration was found to maximize the delay in the coating speed for a stable coating. Romero $et.$ $al.$[2,14] have investigated the impact of viscoelasticity and the evolution mechanism of coating instability through computations and experiments. Their computations indicate that at low Weissenberg numbers, $Wi << 1$, a mild increase in elasticity was found to stabilize coating by decreasing the minimum wet thickness. Whereas at large Weissenberg numbers, $Wi > 1$, strong extensional thickening was found to destabilize the flow resulting in larger minimum wet thickness. The Weissenberg number is defined as the product of the fluid relaxation time, λ, and shear rate imposed, $\dot{\gamma}$. A few studies also exist investigating the effect of shear-thinning on slot-die coating through a combination of experiments, using homogenous blackstrap molasses, and computations[23,24]. An increased shear-thinning behavior was found to maximize the delay on the onset of air entrainment[23].

Literature also exits on slot-die coating of particle dispersions[17,25–27]. Yamamura $et.$ $al.$[17] conducted coating tests on dilute suspensions of poly(methylmethacrylate) (PMMA) particles. They have found that an optimal particle concentration and particle size maximized the critical velocity for the onset of air entrainment. Chu $et.$ $al.$[25], through experiments on suspensions of TiO_2 and SiO_2 in an aqueous polyvinyl alcohol (PVA) solutions have shown that particle concentration, particle size and particle surface texture can have a significant impact on the operating window. Lin $et.$ $al.$[27] investigated the effect of particle size and particle concentration on the operating window using dilute suspensions of poly(methylmethacrylate)

(PMMA) particles in glycerol. When the coating defect is ribbing, the operating window was found to be insensitive to the addition of particles. However, when the coating defect is air entrainment, the particle size and particle concentration was found to strongly influence the operating window.

The studies on slot-die coating of particle dispersions are limited to dilute concentrations with low viscosities ($<<$ 0.5 Pa.s) where the behavior is Newtonian or dispersions that exhibit shear-thinning behavior[17,25,27]. Applications, particularly roll-roll technology for fabrication of broad range of applications, can involve coating of variety of particle dispersions with complex rheology[5]. At sufficiently large concentrations the particle dispersions can potentially shear-thicken[28]. The shear-thickening particle dispersions have also been found to exhibit strong extensional thickening behavior[29–31]. The combination of shear and extensional thickening behavior of the particle dispersions can significantly influence the printing/coating processes[31]. Here we investigate the behavior of shear-thickening coating fluids on the stability of slot-die coating process. The impact of shear-thickening on the operating window was studied by conducting tests on a series of particle dispersions at different concentrations with properties that evolve from Newtonian to shear thinning, and then to shear thickening as the concentration is increased. In addition, the evolution of different coating defects outside the operating window was examined. Finally, the effect of coating gap on the operating window for shear-thickening fluids was studied. In each case, the results were compared with a similar viscosity Newtonian case to understand the importance of complex rheology for these high viscosity liquids.

Methods and Materials

Experimental setup

The slot-die coating experiments were performed on a custom-built lab-scale slot-die coater. The schematic of the slot-die coating experimental set-up is shown in Figure 1. The critical dimensions of the slot die coater geometry in Figure 1 are presented in Table 1. A syringe pump (kd Scientific, model 100) was used to deliver the fluid through the slot-die set vertically downward, with flow rates ranging from 8 to 125 mm^3/s. The coating fluid pumped through the slot-die was coated onto a PET substrate moving horizontally with velocities ranging from 1 mm/s to 25 mm/s using two steel rollers. The evolution and uniformity of the coating was visualized under the die through a high speed camera (Vision Research, Phantom 4.6). The

coated fluid was recovered to recycle using a scraper at far downstream. In order to construct an operating window, the flow rate was held constant and the velocity of the substrate was increased incrementally to identify the critical velocity for the onset of coating defect. The process was repeated for different flow rates and coating gaps.

Test fluids

Our model fluid was fumed silica nanoparticles (Aerosil @200, Evonik Industries; primary particle diameter 20 nm, specific surface area 200 m^2/g) dispersed in polypropylene glycol (PPG) (Aldrich Chemicals, average M.W 1000 g/mol). A series of test fluids with varying concentration (0 wt% to 10 wt%) were prepared by mixing in a blender for an hour until a transparent and colorless dispersion was obtained. The resulting dispersions were kept in the vacuum chamber for several hours to remove the air bubbles before use[29]. The surface tension was measured using a pendant drop tensiometer (Dataphysics OCA 15plus). The surface tension was found to be insensitive to the nanoparticle concentration, and was found to be σ = 30 mN/m. Model fluids for Newtonian cases were silicone oil of viscosities 5 Pa.s (Silcone5) (RT5000, CANNON Instrument Co.) and 30 Pa.s (Silcone30) (VISCO-30M, GE Silicones) of surface tension, σ = 20 mN/m.

Shear rheology

The shear rheology was probed using a stress-controlled TA DHR-3 rheometer using a 40 mm aluminum parallel-plate geometry at a constant temperature of 25°C temperature with a solvent trap to prevent evaporation. The samples were pre-sheared to erase any shear history during sampling preparation and handing[32,33]. After pre-shear, samples were allowed to rest for 4 minutes to reach equilibrium. Steady shear viscosity measurements were conducted in the shear rate range of $0.1 \, \text{s}^{-1} \leq \dot{\gamma} \leq 100 \, \text{s}^{-1}$.

The shear rheology of fumed silica nanoparticle dispersions in PPG with increasing silica concentration from 0 to 10 wt% is shown in Figure 2. The test fluids were all found to be shear thinning at low shear rates. This behavior has been shown to result from the formation of strings of particles aligned along the direction of shear fields[34]. For concentrations above 5 wt% fumed silica, the fluids were found to shear-thicken beyond a critical shear rate. The magnitude of shear-thickening was found to progressively increase with increasing silica concentration from 7.5 wt% to 10 wt%. The mechanism for the shear-thickening

5

behavior of these nanoparticles has been attributed to the formation of large hydrodynamic-induced clusters of nanoparticles[34]. The critical shear rate for the onset of shear rate of shear-thickening was found to decrease from $\dot{\gamma}_c = 7$ s^{-1} to $\dot{\gamma}_c = 4$ s^{-1} with increasing particle concentration. At even larger shear rates ($\dot{\gamma}$ > 50 s^{-1} for 7.5 wt% and $\dot{\gamma}$ > 20 s^{-1} for 10 wt%), the fluids were found to again shear-thin due to yielding of the microstructure at the large applied shear stresses.

Extensional rheology

Elongational viscosity of the test fluids was measured using a capillary breakup extensional rheometer (CaBER), which is typically used to characterize less viscous fluids[35–39]. The CaBER measurements presented here were performed using a high-speed capillary breakup extensional rheometer designed and developed specifically for these experiments. In CaBER experiments, a cylindrical liquid bridge is created between two cylindrical plates and is stretched from an initial length, L_0, to a final length, L_f at a constant velocity. Once the stretch is stopped, the capillary thinning of the liquid bridge formed between the two end plates or uniaxial extensional flow that is resisted by the viscous and elastic stresses developed by the flow within the filament. By monitoring the evolution of the filament diameter as a function of time, the extension rate, $\dot{\varepsilon}$, of the fluid filament is calculated as

$$\dot{\varepsilon} = -\frac{2}{R_{mid}(t)} \frac{dR_{mid}(t)}{dt}. \tag{1}$$

The apparent extensional viscosity, η_E, can be calculated by applying a force balance between capillary stresses and the viscous and elastic tensile stresses within the fluid filament ignoring inertia[38,39] as

$$\eta_{E,app} = \frac{\sigma/R_{mid}(t)}{\dot{\varepsilon}} = \frac{-\sigma}{dD_{mid}(t)/dt}. \tag{2}$$

In the CaBER experiments presented here, the initial and final aspect ratios of the liquid bridge were set as, $\Lambda_0 = 1$ and $\Lambda_f = 3$. Where $\Lambda_0 = L_0/R_0$ and L_0 is the initial separation between the plates. Due to the shear-thickening nature of these dispersions for concentrations above 5 wt%, the initial step stretch is created at slower velocities ranging from 2 to 10 mm/s in order to minimize any influence of any deformation history on the capillary breakup process. The time scales of step stretch are smaller than the viscous breakup time scales, $t_v \sim \eta R_0/\sigma$, to observe capillary thinning[37].

6

In Figure 3, the diameter evolution for a series of particle dispersions in PPG with silica concentrations ranging from 5 wt% to 10 wt% is shown. An increase in the lifetime of the filament was observed with increasing particle concentration indicating an increasing extensional viscosity. The apparent extensional viscosity, η_E, thus calculated using equation 2 is shown as a function of Hencky strain, ε, for various particle concentrations in Figure 4. The corresponding extensional rates, $\dot{\varepsilon}$, calculated from the diameter decay using equation 1 are also shown in the inset. The apparent extensional viscosity at low strains was found to increase with increasing particle concentration as expected. Beyond a certain strain, the extensional viscosity increases indicating extensional thickening of the fluid. This behavior increases with increasing particle concentration. The Trouton ratio at low Hencky strains, $Tr = \eta_{E,0}/\eta_0$, for all particle concentrations is approximately three as expected, $Tr \approx 3$. The effect of particle concentration on extensional thickening is consistent with the observations in literature [29,31,40].

Results and discussion

Newtonian fluids

Prior to investigating the influence of non-Newtonian behavior on slot-die coating process, tests were conducted on three Newtonian fluids; two silicone oils one with a viscosity of $\eta = 5$ Pa.s (Silcone5) and the other with a viscosity of $\eta = 30$ Pa.s (Silcone30) along with pure polypropylene glycol (PPG) with a viscosity of $\eta = 0.15$ Pa.s. The operating window, flow rate versus critical velocity, usually obtained is a closed region, where several coating defects appear outside the window. The lower bound of the operating window, where flooding or dripping is commonly observed, was not possible to observe for most fluids due to experimental difficulties in obtaining velocities lower than 1 mm/s. Therefore, only upper critical velocity, V_c, beyond which a coating defect is observed for different flow rates, was studied. The operating window for the Newtonian fluids are presented in Figure 5. The type of coating defect outside the operating window has also been presented. For all test fluids, as the volume flow rate of fluid through the slot die was increased, the critical web velocities for the onset of a coating defect was found to increase. As the fluid viscosity was increased from $\eta = 0.15$ Pa.s to $\eta = 5$ Pa.s, the critical web velocity for the onset of a coating defect for any given flow rates, was found to decrease by a factor of more than three. Increasing the viscosity further from $\eta = 5$ Pa.s to $\eta = 30$ Pa.s only slightly decreased the critical web velocities. This decrease in

the critical web velocities for the onset of a coating defect with increasing viscosity suggests that the fluid viscosity has a negative impact on the size of the operating window. This behavior is consistent with the literature observations for the case of homogenous Newtonian solutions[9,19,23,27,41–43].

Outside the operating window, a number of different types of coating defects were observed for the three fluids as shown in the images in Figure 6. For the Silicone5 fluid, the coating defect at low web speeds was initially observed to be air entrainment. As the velocity of the web was further increased well beyond the stable coating window a secondary transition from air entrainment to a regular pattern of alternating waves of dry and wet stripes across the web known as a ribbing defect was observed. An image of this ribbing defect is shown in Figure 6c. The critical velocity for the onset of ribbing for different volume flow rates of Silicone5 through the slot die coating head is also shown in Figure 5. For the case of the Silicone30 fluid, which is six times more viscous than Silicone5 fluid, the coating defect were found to evolve as breaklines as shown in the image presented in Figure 6d. Unlike Silicone5 fluid, no ribbing defect was observed at large velocities. However, the defect evolves to air entrainment at large velocities as shown in the Figure 6e. For the low viscosity PPG fluid, the coating defect outside the operating window is a combination of large irregular ribs and isolated dewetting spots as shown in the images in Figure 6e and 6f.

Non-Newtonian fluids

In order to examine the effect of shear-thickening on the operating window, slot-die coating measurements were performed on a series of fumed silica nanoparticle dispersions in PPG with varying silica concentration ranging from 5 to 10 wt%. The volume flow rate of the fluid through the slot-die coater head versus the critical web velocity for the onset of coating defect is shown in Figure 7 for these non-Newtonian test fluids and the pure PPG for reference. For all concentrations, the critical velocity for the onset of defect increased with increasing flow rate. As the particle concentration was increased from 0 wt% up to 7.5 wt%, the critical web velocity was observed to decrease by a factor of more than three. Increasing the particle concentration beyond 7.5 wt% concentration, was found to only slightly decrease the critical web velocity for the onset of defect. The overall decrease in the critical web velocity for the onset of the coating defect with increasing particle concentration at any given flow rate suggests that the addition of particles has a negative impact on the size of the operating window. However, it is important to note that as seen in Figure 2 adding fumed silica particles to PPG increases the viscosity of the fluid. As shown for Newtonian

8

fluids in Figure 5, it is known that increasing the viscosity of the test fluid destabilizes the coating window by reducing the critical web velocity for coating defect to appear. Here the fluids are non-Newtonian and the fluid viscosities are not constant, but depend on the shear-rate within the slot-die and in the coating gap between the slot-die head and the moving web.

The shear rate between the slot-die head and the moving web depends on both the volume flow rate of fluid and the velocity of the moving web. If we assume all the fluid is deposited on the web and none drips off the side of the web, we can derive the following velocity profile

$$u = \frac{6Q}{LH^3}(yH - y^2) + V(1 - \frac{3y}{H})$$

(3)

. From (3) the shear shear rate across the gap can be calculated as

$$\dot{\gamma} = \frac{6Q}{LH^2}(1 - \frac{2y}{H}) + \frac{V}{H}(\frac{y}{H} - 4)$$

(4)

The viscosity $\eta(\dot{\gamma}_{avg})$ of each fluid is presented in Figure 7b evaluated at the average shear rate between the die and the moving web at the critical web velocity and the volume flow rate conditions associated with the onset of coating defect in Figure 7a. This data is presented so that the correlation of fluid viscosity to the trends in operating window can be examined for each different nanoparticle dispersions. For 5 wt% case, the critical shear rate at the onset of the coating defect are well into the high shear rate constant viscosity regime and do not vary much with the web velocity. For the concentration beyond 5 wt%, the critical shear rates at the onset of defect were all well into the shear-thickening regime. At those processing conditions, the 10 wt% case has a viscosity that is more than two orders of magnitude larger than both the 5 wt% case and the pure PPG case. As seen for the Newtonian fluids in Figure 5, increased viscosity is known to reduce the coating window. The question we would like to answer is whether these variation can be explained by increased viscosity alone or whether shear thickening and the variation of fluid viscosity across the gap fundamentally change the stability window and the dynamics of coating defect.

The images of different coating defects presented outside the operating window for the non-Newtonian fluids are shown in Figure 8. As described previously, at zero particle concentration, the coating defect outside the operating window appear as a combination of irregular bands and large dewetted regions or spots

across the web. As the particle concentration was increased, the coating defect evolves to more uniform ribs with periodic patterns of dry and wet regions across the web. This ribbing instability is shown in the images in Figure 8 for the three different particle concentrations. The ribbing instability is one of the most commonly observed defect in coating flows for both Newtonian and viscoelastic fluids[2,44,44–51]. The mechanism of ribbing has been extensively investigated in literature, both theoretically[45,46,52] as well as experimentally[2,44,50]. The ribbing evolution is commonly related to Saffmon-Talyor instabilty, a free surface flow instability where a fluid film splits in multiple films or fibrils due to adverse pressure gradient driven by viscous forces[53]. The evolution of the observed ribbing instability for the 10 wt% shear-thickening fluid is shown in Figure 9 as a series of images with increasing time for a constant volume flow rate and web speed. As the web velocity is increased, the upstream meniscus approaches the feed exit and air fingers evolve from the feed exit. These air fingers propagate further downstream, without breaking up into air pockets, evolving to a periodic array of stable long fluid stripes across the web separated by lanes of dry webbing. This evolution of ribbing is similar to reported by Romero et. al[2] for the case when no vaccum is applied upstream. However, they show that when a vacuum is applied at the upstream, the upstream meniscus is stabilized and the ribbing instability evolves instead from the downstream meniscus with air fingers invading the coating bead.

We have further examined the intensity of the ribbing defect outside the operating window by comparing between different fumed silica concentrations in order to study the sensitivity of the instabilty to the fluids rheology and the strength of the shear-thickening behavior. From Figure 8, it is clear that as the particle concentration is increased, the intensity of the ribbing also increases with, the thickness of the wet ribs decreasing and the number of ribs increasing. These observations can be quantified as a function of web velocity and are compared between 7.5 wt% and 10 wt% concentrations at a fixed volume flow rate and increasing web velocity in Figure 10. The width of the dry and wet ribs and their placement across the web was not completely uniform, as a result error bars which quantify the experiment to experiment fluctuations are placed over the data in Figure 10a. Due to the rib pattern variations across the film, it was determined that the periodicity or wave number of the ribbing was not the appropriate variable to quantify. Instead, we present the number of wet ribs across the web in Figure 10b in addition to the mean thickness of the wet ribs. For both concentrations, with increasing velocity the mean thickness of wet rib was found to decrease while

the number of wet ribs were found to increase. At any given velocity, the mean thickness of the wet ribs is lower for 10 wt% fumed silica dispersion compared to 7.5 wt% case and the number ribs is larger. These observations suggest that increasing shear-thickening behavior maximizes the intensity of ribbing instability by not only driving the instability to lower critical web velocity but by increasing the number of ribs and the rate of change of rib width with increasing web speed.

Previous studies on dilute particle dispersions have reported that, when the coating defect is air entrainment, the addition of particles to a coating fluid, improves the coating window [17,25,27]. However, in the case of fumed silica nanoparticle dispersions in PPG, the coating defect is ribbing, which occurs by a different mechanism compared to air entrainment. Air entrainment is most commonly associated with a failure of dynamic wetting contact line [23,43,54]. Lin et al. [27] have examined the influence of particle addition when the coating defect was ribbing. The addition of particles was not found to have any significant impact on operating window, however the observations were based on limited range of particle concentrations. In all their experiments the viscosity was quite low and Newtonian. Here shear thickening plays a significant role in the stability of the coating.

One way to clearly see the effect of non-Newtonian viscosity on the stability of slot die coating is to study the operating window by plotting the minimum wet thickness, t, as a function of the dimensionless capillary number, $Ca = \eta V_c/\sigma$. The capillary number is the dimensionless ratio of viscous to capillary forces. For the non-Newtonian nanoparticle dispersions, the shear-rate-dependent viscosity, $\eta(\dot{\gamma})$, will be used to evaluate the viscosity where $\dot{\gamma}$ will be the average shear rate given in Equation 4. As a result, $Ca = \eta(\dot{\gamma})V_c/\sigma$. The minimum wet thickness is calculated from conservation of mass to be, $t = Q/(V_cL)$, where L is the length of the die. The wet film thickness is commonly normalized with coating gap to form a dimensionless film thickness, $t_N = t/H$. The normalized minimum wet thickness, t_N, as a function of capillary number is presented in Figure 11 for all three particle dispersions and the Newtonian silicone fluids which were chosen because they had similar viscosities. At low capillary number regime, $Ca \ll 1$, where capillary forces are important compared to viscous forces, the minimum wet thickness was found to increase with capillary number. For the Newtonian fluid the data scale like $t_N \sim Ca^{0.5}$. The scaling exponent is in agreement with that reported for homogenous Newtonian fluids, which is $n \sim 0.5$ - 0.7 at low capillary number regime [6,11,18,19].

However, what is clear for this low capillary number data is that the shear thinning of the 5 wt% solution has a clear detrimental effect on the coating stability. Due to shear thinning, a thin film cannot be easily deposited on the web. As seen in Figure 11, a film with a minimum coating thickness that is nearly twice large as that of the Newtonian fluid can only be deposited before the film becomes unstable. This is dramatic increase that only becomes evident when the effect of viscosity is removed by plotting the data as a function of shear rate dependent capillary number. For the larger capillary number regimes the particle concentrations in the dispersions are greater than > 7.5 wt% and shear thickening of the viscosity is observed. With increasing capillary number, the relative importance of viscous forces compared to capillary forces increases. As can be seen in Figure 11, the results in the high capillary number regime for Newtonian fluids show that the minimum wet thickness is not strongly dependent on capillary number. In this capillary number regime, the value of the normalized film thickness increases slowly from $t_N = 0.44$ to $t_N = 0.55$. This behavior is consistent with the high capillary number limit observed for Newtonian fluids in the past[6,10–12]. Note now that unlike the 5 wt% shear-thinning case for which the complex fluid rheology destabilized the coating, for the shear-thickening fluids, once the effects of Newtonian viscosity increase is accounted for through the shear rate-dependent capillary number, shear thickening appears to stabilize the coating window. For the 10 wt% solution, this corresponds to a reduction in minimum coating wet film thickness of 12 % on average for a given capillary number. For the 7.5 wt% system, the wet film thickness is decreased by 8 % due to shear thickening. The deviation in the case of shear-thinning and shear-thickening fluids, compared to Newtonian fluids, suggests that the viscosity variation of the fluid associated with changes in local shear rates across the coating gap, can have an important influence on the stability of the coating.

Effect of coating gap

As seen in Figure 2 the shear-thickening fluids used here have quite a complex rheology. They shear-thin at low shear rates, shear thicken at moderate shear rates and shear thin again at large shear rates. By varying the coating gap, the range of experimentally accessible shear rates can be varied as seen in Equation 4 while simultaneously studying the impact of coating gap. Here we focused the gap dependent tests on the 10 wt% solution and the 30 Pa.s silicone oil for a range of coating gaps between 0.1 and 1 mm. The operating window constructed for the both the fluids is shown in Figure 12a. For both the Newtonian and non-Newtonian fluids the critical velocities for the onset of defect was found to increase with decreasing

12

the coating gap. This was consistent for all flow rates tested. This observation demonstrates that decreasing the coating gap allows one to deposit thinner films on the web and work at much higher speeds there by expanding the operating window. For the Newtonian fluid, the coating defects outside the operating window at all gaps were found to be breaklines. The effect of coating gap on the operating window for Newtonian fluids is consistent with reported in literature for the case of Newtonian fluids[10,11,41].

The effect of coating gap on the shear-thickening fluid shown in Figure 12a was found to be slightly more profound than for the Newtonian fluid. At the largest coating gap, $H = 1$ mm, the critical web velocities were found to be lower, by as much as 7%, for the 10 wt% shear-thickening fluid compared to the Newtonian oil. However, as the coating gap was decreased to 0.5 mm and below, the impact on the critical web velocities was found to change sign and the critical velocity became larger than that measured for the Newtonian fluid resulting in films with smaller minimum wet thickness. In fact, for the $H = 0.1$ mm gap, the critical web velocity was measured to be 18% larger for the shear-thickening fluid compared to Newtonian fluid. Further, the type of coating defect observed beyond the critical web speed was also found to be sensitive to the coating gap. The images of the coating defect outside the operating window for the 10 wt% shear-thickening fluid at different gaps are show in Figure 13. For coating gaps equal to $H = 0.25$ mm and below, the coating defect was found to be ribbing. While for coating gaps of $H \geq 0.5$ mm the coating defect was found to air entrainment. Note that for the Newtonian fluid, the coating defect at all gaps was found to be breaklines.

Additionally, the minimum wet thickness as a function of capillary number at different coating gaps was also studied for both Newtonian and 10 wt% shear-thickening fluid and is presented in Figure 14. The capillary number was calculated using a shear-rate-dependent viscosity, $\eta(\dot{\gamma})$, where the average shear-rate in coating gap, $\dot{\gamma}_c$, was given in Equation 4. At all gaps, for both shear-thickening and Newtonian fluid, the minimum wet thickness did not change significantly with increasing capillary number. With decreasing coating gap from $H = 1$ mm to 0.1 mm the minimum wet thickness was found to decrease for both shear-thickening and Newtonian fluids. This observation is consistent with the reported in literature for Newtonian fluids[7,11]. For coating gaps below $H = 1$ mm, the minimum wet thickness of shear-thickening fluid was similar to the Newtonian fluids at lower capillary numbers and slightly lower by as much as 8 % at higher capillary numbers. This is quite different from $H = 1$ mm coating gap, where the minimum wet thickness of

shear-thickening fluid was found to be larger than the Newtonian fluid by approximately 8 %. Furthermore, because the average shear-rates within coating gap for the $H = 1$ mm placed the the viscosity well within the shear-thinning regime, the resulting capillary number calculated for the shear-thickening fluid appears shifted to a lower capillary number by more than an order of magnitude than the Newtonian fluid.

One explanation for the disagreement in the critical capillary number between Newtonian and shear-thickening fluid for the $H = 1$ mm coating gap could be that we are using inappropriate shear rate to evaluate the shear rate dependent viscosity. The fluids are also sheared within the slot-die geometry prior to being ejected into the coating gap. The apparent shear-rates in the slot gap is given by Hagen–Poiseuille flow as, $\dot{\gamma}_g = 6Q/(WL^2)$[55]. For the thin coating gap experiments, this shear rate is much smaller than the shear rate between the die and the moving web. As a result, the effect of pre-shear in the slot gap can be ignored. For the $H = 1$ mm gap, the shear rates in the die are quite large and dominate the coating dynamics. The viscosity based on the shear-rates calculated based on slot die gap, $\eta(\dot{\gamma}_g)$, and the coating gap, $\eta(\dot{\gamma}_c)$, are shown in Figure 12b for $H = 1$ mm gap. As seen in Figure 12b for a coating gap of $H = 1$ mm, the shear-rates calculated in the slot gap, $\eta(\dot{\gamma}_g)$, were found to be in the shear-thickening regime while the shear-rate dependent viscosity in the coating gap, $\eta(\dot{\gamma}_c)$, was found to be in the shear-thinning regime. Thus the fluid exiting the slot die has thickened and as it passes through the coating gap it will thin with time and accumulated strain by more than an order of magnitude. The capillary number calculated based on shear-rate dependent viscosity in the slot gap, $\eta(\dot{\gamma}_g)$, is overlayed onto Figure 14 for a coating gap of $H = 1$ mm. The data is shifted to much larger capillary numbers, close to the Newtonian cases which suggests $\eta(\dot{\gamma}_c)$ is the appropriate viscosity to use when calculating the capillary number in this case. Finally note that for the $H = 1$ mm gap case the minimum wet thickness is larger for shear-thickening case compared to Newtonian fluid. This is similar to the observations for shear thinning fluids as seen in Figure 11. This makes some intuitive sense. For shear thinning fluids the viscosity is lowest at the walls where the shear rate is highest and the viscosity is largest in the middle of the flow where the shear rate goes to zero. This viscosity variation leads to destabilization. The variation in viscosity for a shear thickening fluid is inverted with maximum viscosity along the walls. The result is a flow stabilization. For the case where the fluid shear thickens in the die, the viscosity distribution in the coating gap will be similar to the shear thinning fluid with the maximum viscosity in the middle of the flow and lower viscosity near the wall. This is because the fluid enters the

coating gap at high viscosity. The fluid near the walls experiences a lower shear rate and thins. The fluid at the center is not sheared. As a result, its viscosity decays quite slowly, remaining high as it passes through the coating gap.

Conclusions

We have investigated the impact of non-Newtonian behavior, namely shear-thinning and shear-thickening, on the slot die coating process. A model shear-thickening fluid, fumed silica nanoparticles dispersed in polypropylene glycol, was used. The dispersions exhibit shear and extensional thickening behaviors characterized through steady shear and capillary break-up measurements. A series of particle dispersions with concentrations ranging upto 10 wt% was studied. Three Newtonian fluids were also tested for comparison with shear-thickening fluids. The critical web velocity for the onset of coating defect for different flow-rates was measured. And the type of coating defect outside the operating was visualized through high speed camera. With increasing the particle concentration, the critical web velocity for the onset of coating defect was found to decrease for any given volume flow rate of the fluid, suggesting that shear-thickening of the fluid has a negative impact on the size of the operating window. At all concentrations, the coating instability was found to be ribbing. The ribbing instability was found to evolve from upstream of the coating bead between the slot-die and the substrate. The intensity of ribbing instability was found to increase with increasing shear-thickening magnitude or the particle concentration. The minimum wet thickness as a function of capillary number was also studied. A deviation in the minimum wet thickness behavior was observed when compared between non-Newtonian and Newtonian fluids. The shear-thinning fluid was found to destabilize coating resulting in a larger minimum wet-thickness, conversely shear-thickening resulted in a smaller minimum wet thickness compared to Newtonian cases and a stabilized coating. The effect of shear-thickening was additionally examined by conducting tests with varying coating gap. For both Newtonian and shear-thickening cases, increasing coating gap delayed the critical web velocity for onset of the coating web and resulted in smaller minimum wet thickness. From tests at different coating gaps, the coating stability for shear-thickening fluids was found to be more sensitive to coating gap than Newtonian fluid. At very large gaps, the stability of the coating was found to be affected by the shear thickening of the fluid in slot die gap prior to entering coating gap. The shear-thickening of the fluid in the coating gap was found to stabilize the

15

coating resulting in smaller minimum wet thickness compared to coatings of Newtonian fluids. Conversely, shear-thinning in the coating gap was found to destabilize the coating resulting in a larger minimum wet thickness compared to Newtonian case. The study demonstrates that the non-Newtonian behavior can significantly impact the stability of the slot-die coating process beyond what can be accounted for by simply normalizing the data with the appropriate capillary number.

References

[1] Beguin AE. Method of Coating Strip Material. 1954; US Patent No. 2,681,294.

[2] Romero OJ, Suszynski WJ, Scriven LE, Carvalho MS. Low-flow limit in slot coating of dilute solutions of high molecular weight polymer. *J Non-Newtonian Fluid Mech*. 2004;118(2–3):137 – 156.

[3] Krebs FC. Fabrication and processing of polymer solar cells: A review of printing and coating techniques. *Sol Energy Mater Sol Cells*. 2009;93(4):394 – 412.

[4] Sandström A, Dam HF, Krebs FC, Edman L. Spraying Light: Ambient-Air Fabrication of Large-Area Emissive Devices on Complex-Shaped Surfaces. *Nat Commun*. 2012;3:1002.

[5] Schmitt M, Baunach M, Wengeler L, Peters K, Junges P, Scharfer P, Schabel W. Slot-die processing of lithium-ion battery electrodes—Coating window characterization. *Chem Eng Process*. 2013;68:32 – 37.

[6] Ruschak KJ. Limiting flow in a pre-metered coating device. *Chem Eng Sci*. 1976;31(11):1057 – 1060.

[7] Ning CY, Tsai CC, Liu TJ. The effect of polymer additives on extrusion slot coating. *Chem Eng Sci*. 1996;51(12):3289 – 3297.

[8] Lin CF, Hill Wong DS, Liu TJ, Wu PY. Operating windows of slot die coating: Comparison of theoretical predictions with experimental observations. *Adv Polym Tech*. 2010;29(1):31–44.

[9] Gutoff EB, Kendrick CE. Low flow limits of coatability on a slide coater. *AIChE J*. 1987;33(1):141–145.

[10] Chang YR, Chang HM, Lin CF, Liu TJ, Wu PY. Three minimum wet thickness regions of slot die coating. *J Colloid Interf Sci*. 2007;308(1):222 – 230.

[11] Lee KY, Liu LD, Ta-Jo L. Minimum wet thickness in extrusion slot coating. *Chem Eng Sci*. 1992; 47(7):1703 – 1713.

[12] Higgins BG, Scriven LE. Capillary pressure and viscous pressure drop set bounds on coating bead operability. *Chem Eng Sci*. 1980;35(3):673 – 682.

[13] Carvalho MS, Kheshgi HS. Low-flow limit in slot coating: Theory and experiments. *AIChE J*. 2000; 46(10):1907–1917.

[14] Romero OJ, Scriven LE, Carvalho MS. Slot coating of mildly viscoelastic liquids. *J Non-Newtonian Fluid Mech*. 2006;138(2–3):63 – 75.

[15] Bajaj M, Bhat PP, Prakash JR, Pasquali M. Multiscale simulation of viscoelastic free surface flows. *J Non-Newtonian Fluid Mech*. 2006;140(1–3):87 – 107.

[16] Bajaj M, Prakash JR, Pasquali M. A computational study of the effect of viscoelasticity on slot coating flow of dilute polymer solutions. *J Non-Newtonian Fluid Mech*. 2008;149(1–3):104 – 123.

[17] Yamamura M, Miura H, Kage H. Postponed air entrainment in dilute suspension coatings. *AIChE J*. 2005;51(8):2171–2177.

[18] Yang CK, Wong DSH, Liu TJ. The effects of polymer additives on the operating windows of slot coating. *Polym Eng Sci*. 2004;44(10):1970–1976.

[19] Lin FH, Liu CM, Liu TJ, Wu PY. Experimental study on tensioned-web slot coating. *Polym Eng Sci*. 2007;47(6):841–851.

[20] Chang HM, Lee CC, Liu TJ. The Effect of Bead Vacuum on Slot Die Coating. *Int Polym Proc*. 2009; 24(2):157 – 165.

[21] Lee AG, Shaqfeh ES, Khomami B. A study of viscoelastic free surface flows by the finite element method: Hele–Shaw and slot coating flows. *J Non-Newtonian Fluid Mech*. 2002;108(1–3):327 – 362.

[22] Pasquali M, Scriven LE. Free surface flows of polymer solutions with models based on the conformation tensor. *J Non-Newtonian Fluid Mech*. 2002;108(1–3):363 – 409.

[23] Bhamidipati KL. Detection and elimination of defects during manufacture of high-temperature polymer electrolyte membranes. Ph.D. thesis, Georgia Institute of Technology. 2011.

[24] Didari S, Ahmad Z, Veldhorst J, Harris T. Wetting behavior of the shear thinning power law fluids. *J Coat Technol Res*. 2014;11(1):95–102.

[25] Chu WB, Yang JW, Wang YC, Liu TJ, Tiu C, Guo J. The effect of inorganic particles on slot die coating of poly(vinyl alcohol) solutions. *J Colloid Interf Sci*. 2006;297(1):215 – 225.

[26] Chu WB, Yang JW, Liu TJ, Tiu C, Guo J. The effects of pH, molecular weight and degree of hydrolysis of poly(vinyl alcohol) on slot die coating of PVA suspensions of TiO2 and SiO2. *Colloids Surf A Physicochem Eng Asp*. 2007;302(1–3):1 – 10.

[27] Lin YT, Chu WB, Liu TJ. Slot die coating of dilute suspensions. *Asia-Pacific J Chem Eng*. 2009; 4(2):125–132.

[28] Barnes HA. Shear-Thickening ("Dilatancy") in Suspensions of Nonaggregating Solid Particles Dispersed in Newtonian Liquids. *J Rheol*. 1989;33:329–366.

[29] Chellamuthu M, Arndt EM, Rothstein JP. Extensional rheology of shear-thickening nanoparticle suspensions. *Soft Matter*. 2009;5:2117–2124.

[30] Khandavalli S, Rothstein J. Extensional rheology of shear-thickening nanoparticle dispersions in an aqueous polyethylene oxide solutions. *J Rheol*. 2014;58(2):411–431.

[31] Khandavalli S, Lee JA, Pasquali M, Rothstein JP. The effect of shear-thickening on liquid transfer from an idealized gravure cell. *J Non-Newtonian Fluid Mech*. 2015;221:55 – 65.

[32] Raghavan SR, Khan SA. Shear-induced microstructural changes in flocculated suspensions of fumed silica. *J Rheol*. 1995;39(6):1311–1325.

[33] Galindo-Rosales FJ, Rubio-Hernàndez FJ. Static and dynamic yield stresses of Aerosil®200 suspension in polypropylene glycol. *App Rheol*. 2010;20:22787.

[34] Wagner NJ, Brady JF. Shear thickening in colloidal dispersions. *Physics Today*. 2009;62(10):27–32.

[35] Entov VM, Hinch EJ. Effect of a spectrum of relaxation times on the capillary thinning of a filament of elastic liquid. *J Non-Newtonian Fluid Mech*. 1997;72:31–53.

[36] Bhardwaj A, Miller E, Rothstein JP. Filament stretching and capillary breakup extensional rheometry measurements of viscoelastic wormlike micelle solutions. *J Rheol*. 2007;51(4):693–719.

[37] Rodd LE, Scott TP, Cooper-White JJ, McKinley GH. Capillary break-up rheometry of low-viscosity elastic fluids. *Appl Rheol*. 2005;15(1):12–27.

[38] Anna SL, McKinley GH. Elasto-capillary thinning and breakup of model elastic liquids. *J Rheol*. 2001;45(1):115–138.

[39] Papageorgiou DT. On the breakup of viscous liquid threads. *Phys Fluids*. 1995;7:1529–1544.

[40] Wang J, Bai R, Joseph DD. Nanoparticle-laden tubeless and open siphons. *J Fluid Mech*. 2004; 516:335–348.

[41] Chang HM, Chang YR, Lin CF, Liu TJ. Comparison of vertical and horizontal slot die coatings. *Polymer Engineering Science*. 2007;47(11):1927–1936.

[42] Veverka PJ. An investigation of interfacial instability during air entrainment . Ph.D. thesis, University of Delaware. 1988.

[43] Burley R, Kennedy BS. An experimental study of air entrainment at a solid/liquid/gas interface. *Chem Eng Sci*. 1976;31(10):901 – 911.

[44] Zevallos G, Carvalho M, Pasquali M. Forward roll coating flows of viscoelastic liquids. *J Non-Newtonian Fluid Mech*. 2005;130(2–3):96 – 109.

[45] Gokhale VV. Bounds for Region of Ribbing Instability in Some Free Surface Coating Flows. *J Rheol*. 1981;25(4):421–432.

[46] Carvalho MS, Scriven LE. Flows in Forward Deformable Roll Coating Gaps: Comparison between Spring and Plane-Strain Models of Roll Cover. *J Comput Phys*. 1997;138(2):449 – 479.

[47] López FV, Pauchard L, Rosen M, Rabaud M. Non-Newtonian effects on ribbing instability threshold. *J Non-Newtonian Fluid Mech*. 2002;103(2–3):123 – 139.

[48] Bauman T, Sullivan T, Middleman S. Ribbing instability in coating flows: effect of polymer additives. *Chem Eng Commun*. 1982;14(1-2):35–46.

[49] Dontula P. Polymer solutions in coating flows. Ph.D. thesis, University of Minnesota. 1999.

[50] Gaskell PH, Kapur N, Savage MD. Bead-break instability. *Physics of Fluids*. 2001;13(5):1243–1253.

[51] Benkreira H, Edwards MF, Wilkinson WL. Roll coating of purely viscous liquids. *Chem Eng Sci*. 1981;36(2):429 – 434.

[52] Castillo MEG, Patera AT. Three-dimensional ribbing instability in symmetric forward-roll film-coating processes. *J Fluid Mech*. 1997;335:323–359.

[53] Graham MD. Interfacial hoop stress and instability of viscoelastic free surface flows. *Physics of Fluids*. 2003;15(6):1702–1710.

[54] Deryagin BV, Levi SM. *Film Coating Theory*. Focal Press London. 1959.

[55] Papanastasiou T, Georgiou G, Alexandrou AN. *Viscous Fluid Flow*. CRC Press. 1999.
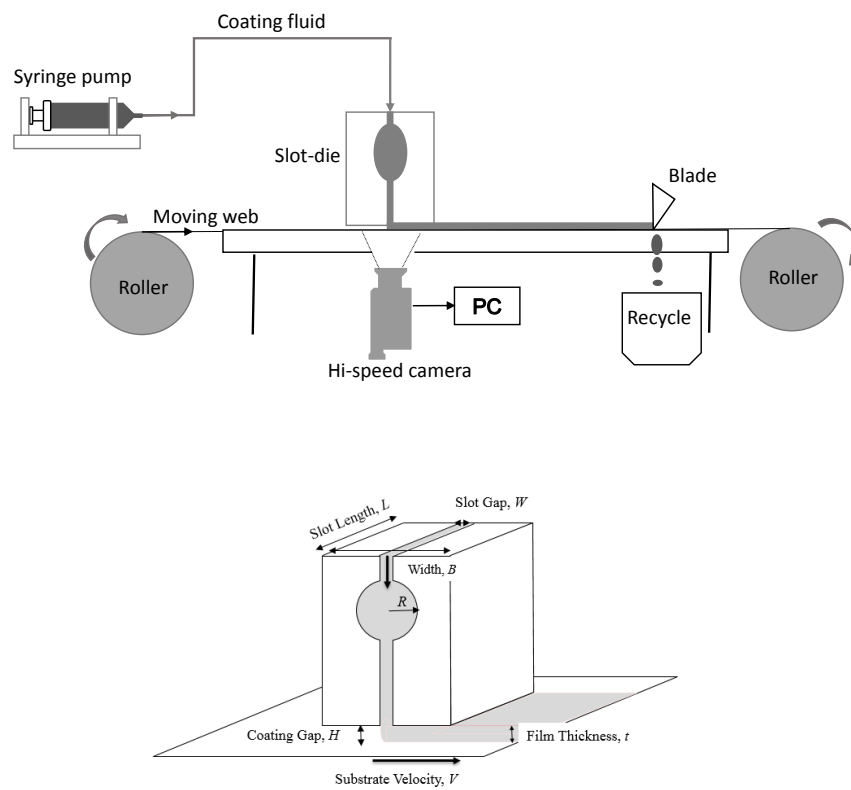
Figure 1: Schematic of slot-die coating experimental set-up

Table 1: Slot-die parameters and range of experimental operating parameters.

Die parameters	Dimensions
Die length (L)	48 mm
Die width (B)	24 mm
Slot gap width (W)	0.50 mm
Coating gap (H)	0.1 - 1.0 mm
Cavity radius (R)	4.7 mm
Substrate velocity (V)	1.0 - 25.0 mm/s
Pump flow rate (Q)	8 - 125 mm^3/s
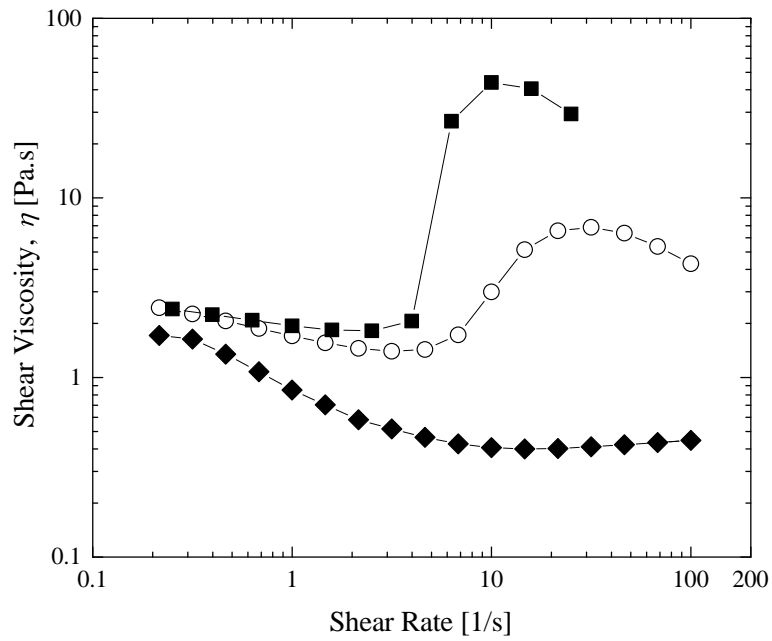
Figure 2: Steady shear viscosity as a function of shear rate for a series of fumed silica dispersions in PPG. The data include a series of particle concentrations: (♦) 5.0 wt%, (○) 7.5 wt% and (■) 10 wt%.
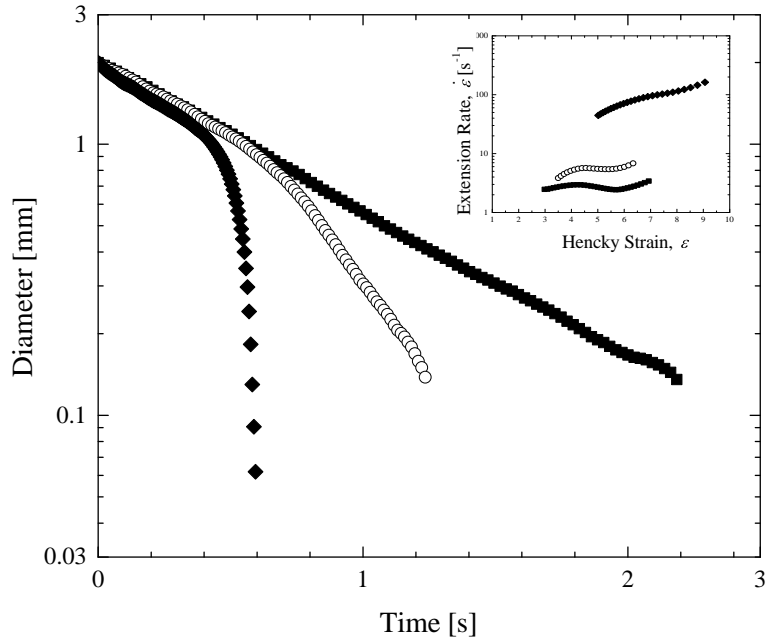
Figure 3: Diameter evolution as a function of time during a capillary breakup extensional rheology measurement for a series of fumed silica dispersions in PPG. The data include a number of different particle concentrations: (◆) 5.0 wt%, (○) 7.5 wt% and (■) 10 wt%. The corresponding plots of extension rate versus Hencky strain for the particle dispersions are shown in the inset.
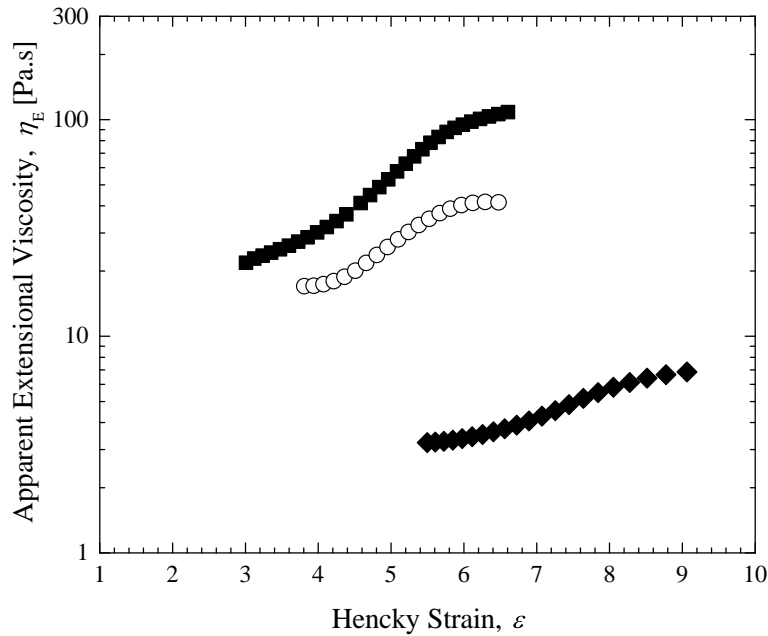
Figure 4: Apparent extensional viscosity as a function of Hencky strain for a series of fumed silica dispersions in PPG. The data include several different particle concentrations: (◆) 5.0 wt%, (○) 7.5 wt% and (■) 10 wt%.
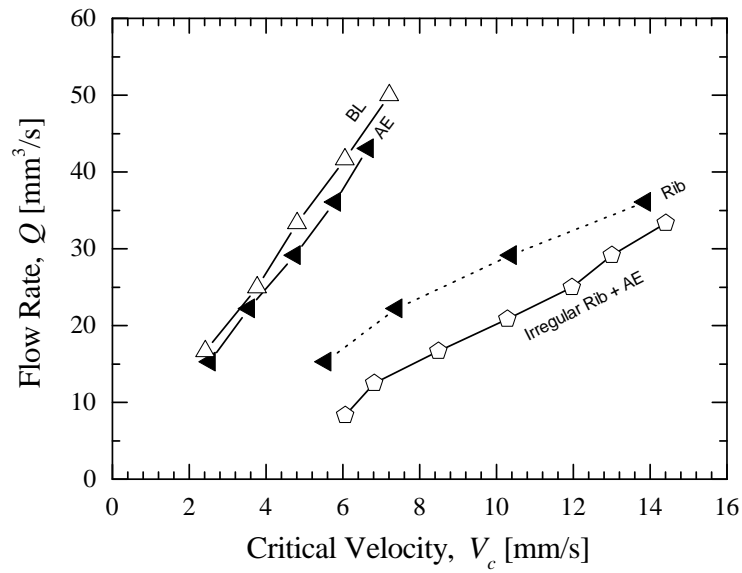
Figure 5: Flow rate, Q versus critical velocity for the onset of defect, V_c, for different Newtonian fluids at a coating gap of 0.25 mm. The test fluids include (⬠) PPG ($\eta = 0.15Pa.s$), (◀) silicone oil ($\eta = 5$ Pa.s) and (△) silicone oil ($\eta = 30$ Pa.s). The dotted line for silicon oil of 5 Pa.s represents the second critical velocity of the onset of ribbing defect. The coating defects beyond the critical velocities are labeled as AE for air entrainment, BL for breaklines and Rib for ribbing.
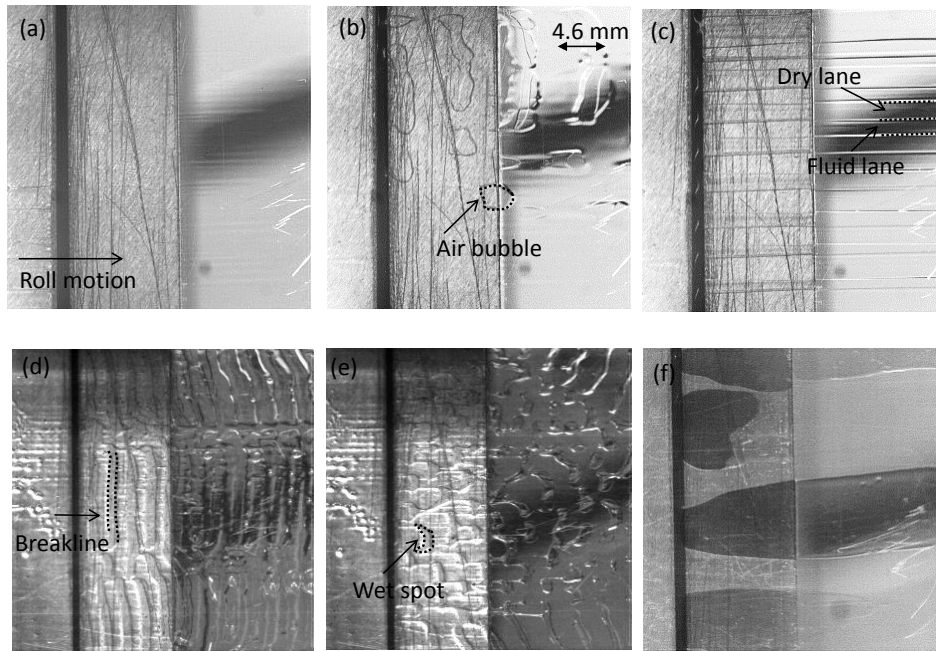
Figure 6: Images of coating for different Newtonian test fluids outside the operating window at a coating gap of 0.25 mm. The images include a) stable coating of 5 Pa.s silicone oil at Q = 30.5 mm^3/s, V = 3.2 mm/s , b) air entrainment defect for 5 Pa.s silicone oil at Q = 30.5 mm^3/s, V = 5.7 mm/s, c) ribbing defect for 5 Pa.s silicone oil at Q = 30.5 mm^3/s, V = 11.8 mm/s, d) breaklines defect in 30 Pa.s silicone oil at Q = 24.9 mm^3, V = 4.1 mm/s e) air entrainment defect in 30 Pa.s silicone oil at Q = 24.9 mm^3, V = 4.8 mm/s and, f) irregular ribbing and air entrainment in PPG at Q = 22.2 mm^3/s, V = 11.6 mm/s.
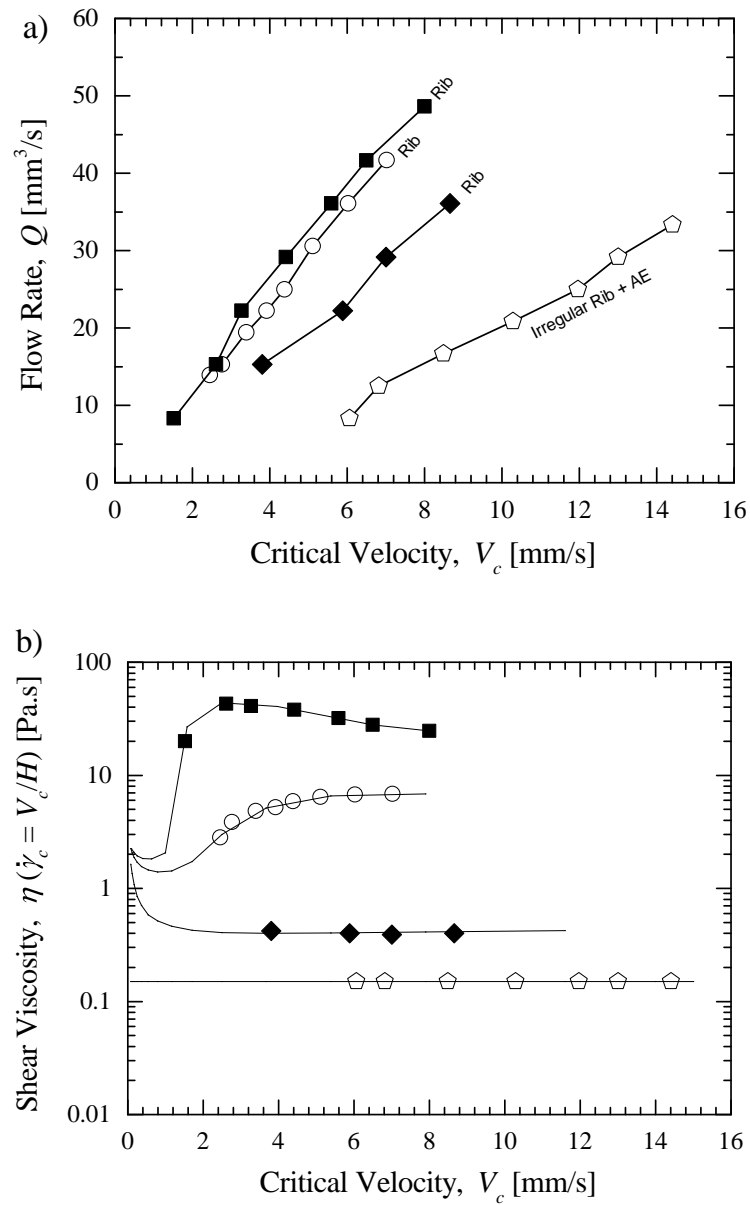
Figure 7: a) Flow rate, Q versus critical velocity for the onset of defect, V_c and b) viscosity, $\eta(\dot{\gamma}_c = V_c/H)$, versus critical velocity for the onset of coating defect, V_c for a series of fumed silica dispersions in PPG at a coating gap of 0.25 mm. The data include a series of particle concentrations: (⬠) 0 wt%, (♦) 5.0 wt%, (○) 7.5 wt% and (■) 10 wt%. Symbols correspond to the data points presented in the operating window for different particle concentrations. The coating defects beyond the critical velocities are labeled as AE for air entrainment and Rib for ribbing.
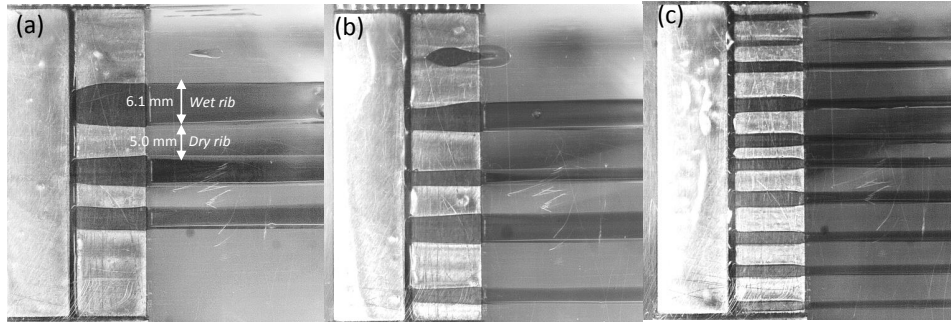
Figure 8: Images of ribbing defect for a series of fumed silica dispersions in PPG outside the operating window for a coating gap of 0.25 mm. The images include for particle concentrations of a) 5 wt% at $Q = 22.2$ mm^3/s, $V = 12.7$ mm/s b) 7.5 wt% at $Q = 22.2$ mm^3/s, $V = 14.4$ mm/s and c) 10 wt% $Q = 22.2$ mm^3/s, $V = 13.5$ mm/s.
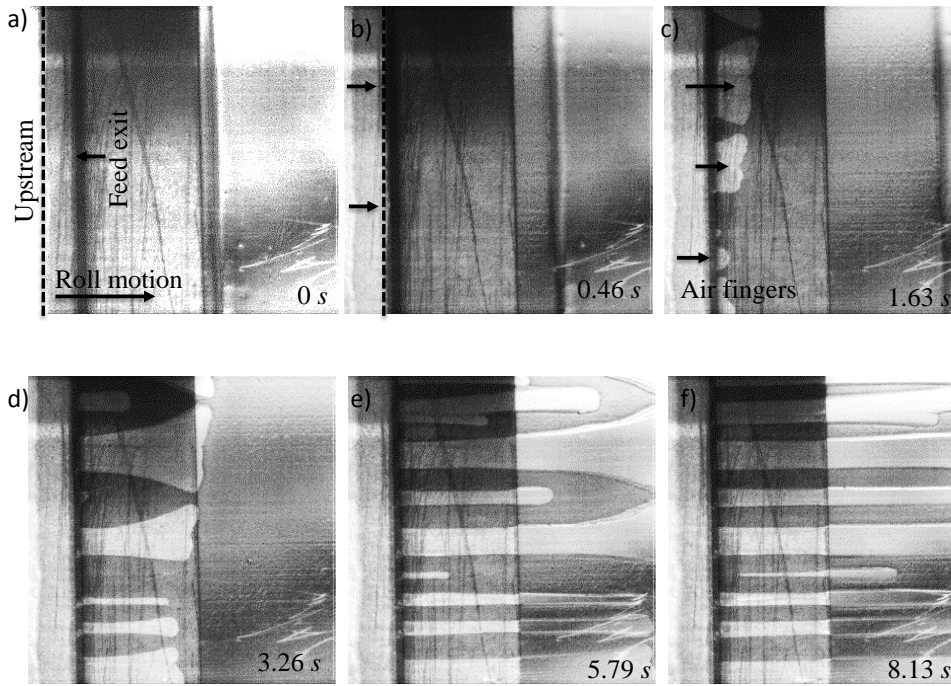
Figure 9: Time series of images of evolution of the ribbing instability of 10 wt% silica in PPG dispersions at a flow rate of 16.6 mm^3/s and web speed of 6.5 mm/s at a coating gap of 0.1 mm. The images include a) stable coating at t = 0 s b) the upstream meniscus approaching the feed exit at $t = 0.46$ s, c-f) air fingers evolution at feed exit and propagation as ribbing downstream for $t > 1.63$ s.

27
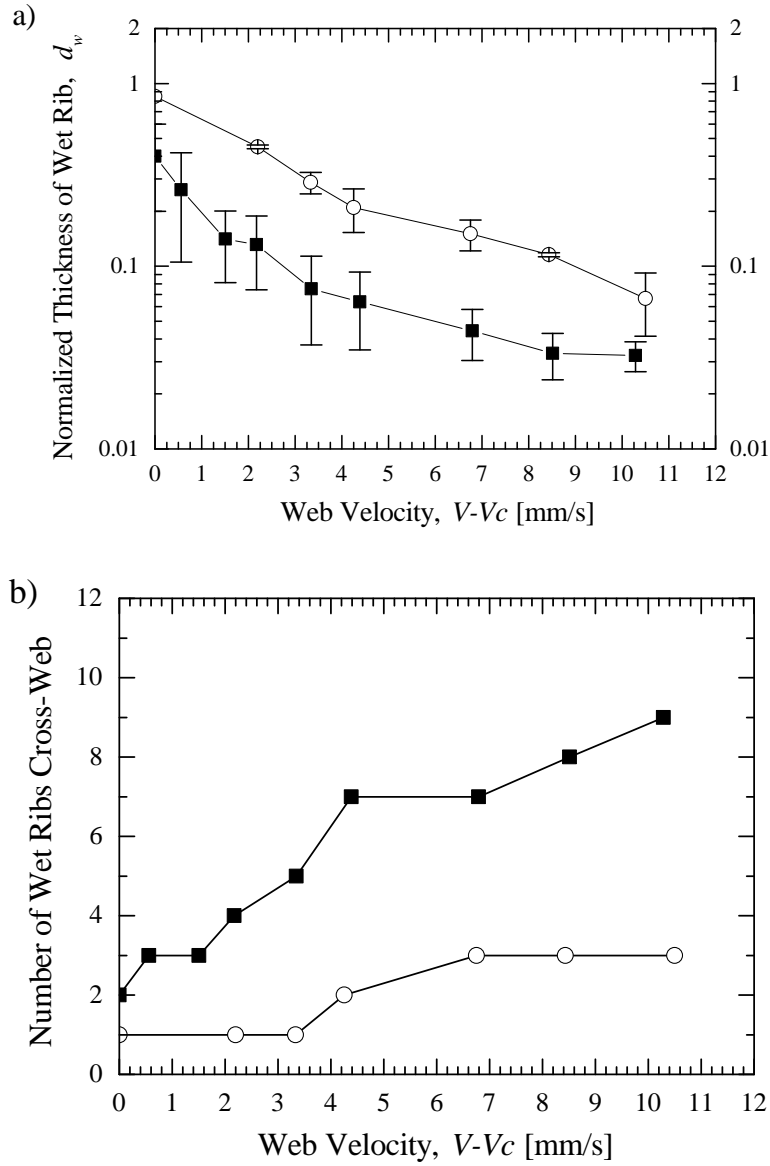
Figure 10: Ribbing defect parameters, a) normalized mean thickness of the wet rib, $d_w = d/L$, and b) number of wet ribs across the web, as a function of web velocity, $V - V_c$, at a flow rate of 22.2 mm^3/s for (○) 7.5 wt% and (■) 10 wt% fumed silica dispersion in PPG.
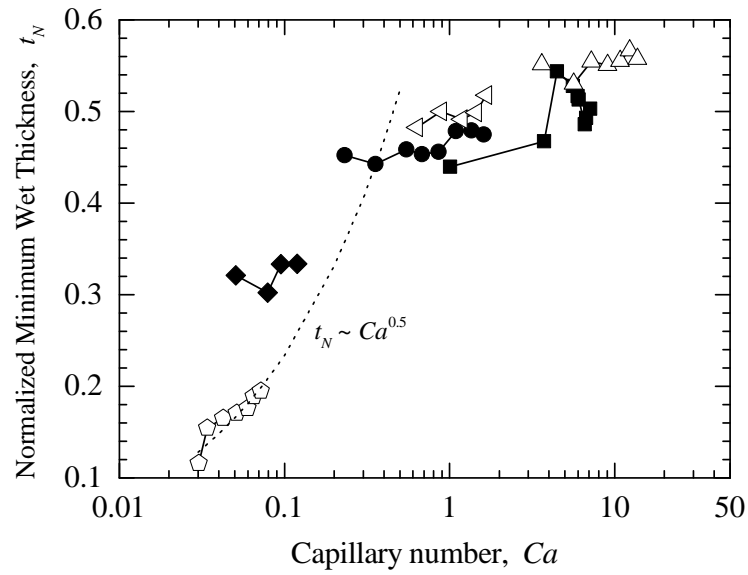
28

Figure 11: Normalized minimum wet thickness, t_N, as a function of capillary number, Ca, for a series of test fluids. The data include a series of fumed silica dispersions in PPG with different particle concentrations: (△) 0 wt%, (♦) 5.0 wt%, (○) 7.5 wt% and (■) 10 wt%. The data for Newtonian silicone oils of viscosities (◂) η = 5 Pa.s and (▲) η = 30 Pa.s is also included. The capillary number is evaluated as, Ca = $\eta(\dot{\gamma}_c)V_c/\sigma$, where $\dot{\gamma}_c = V_c/H$. The dotted line is a power law fit for Newtonian fluid which scales as $t_N \sim Ca^{0.5}$.
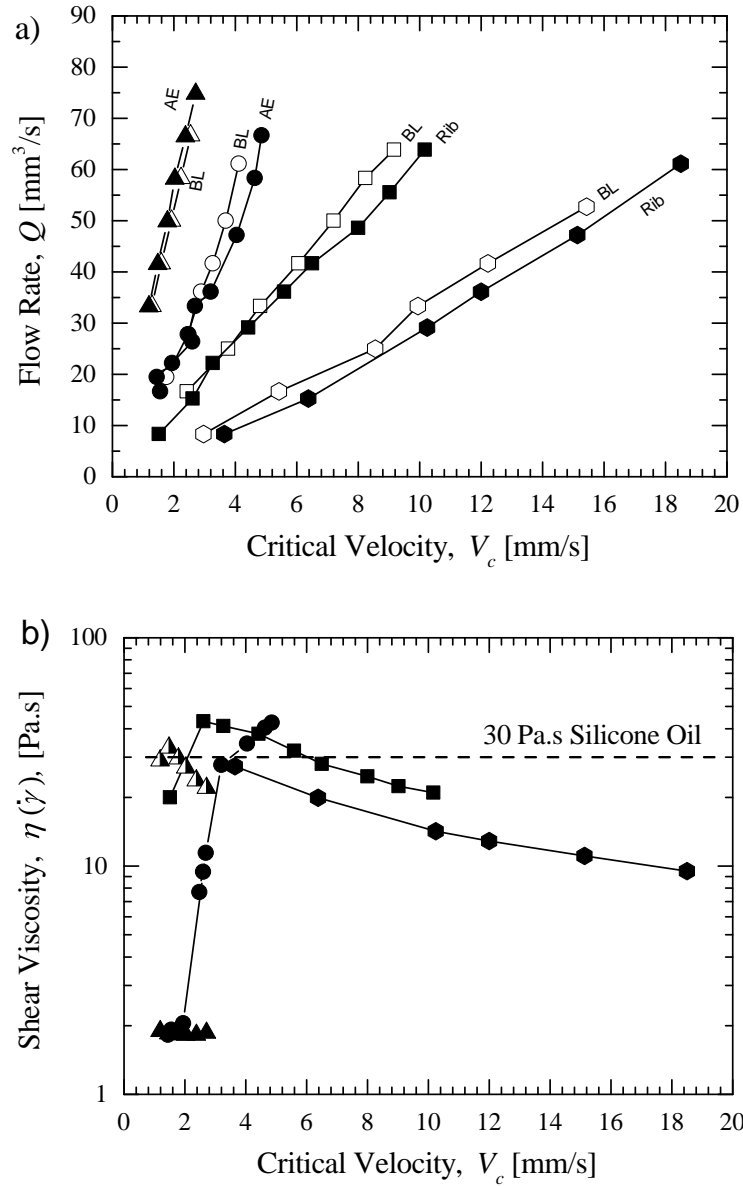
Figure 12: a) Flow rate, Q, versus critical velocity for the onset of defect, V_c, for 10 wt% fumed silica dispersion in PPG (filled symbols) and silicone oil with $\eta = 30$ Pa.s (hollow symbols) at different coating gaps and b) Shear viscosity, $\eta(\dot{\gamma})$ versus critical velocity for the onset of defect, V_c, for 10 wt% fumed silica dispersion in PPG for different coating gaps. The data include for different coating gaps: (○) 0.1 mm, (■) 0.25 mm, (●) 0.5 mm and (▲) 1 mm. The viscosity evaluated based on shear-rate in coating gap given by $\dot{\gamma}_c = V_c/H$ is shown in filled in symbols and for viscosity evaluated based on shear-rate in slot-gap given as $\dot{\gamma}_g = 6Q/(LW^2)$ for 1 mm coating gap is shown in half shaded symbols, where W and L are slot-gap width and slot-die length. The coating defects beyond the critical velocities are labeled as AE for air entrainment, BL for breaklines and Rib for ribbing.
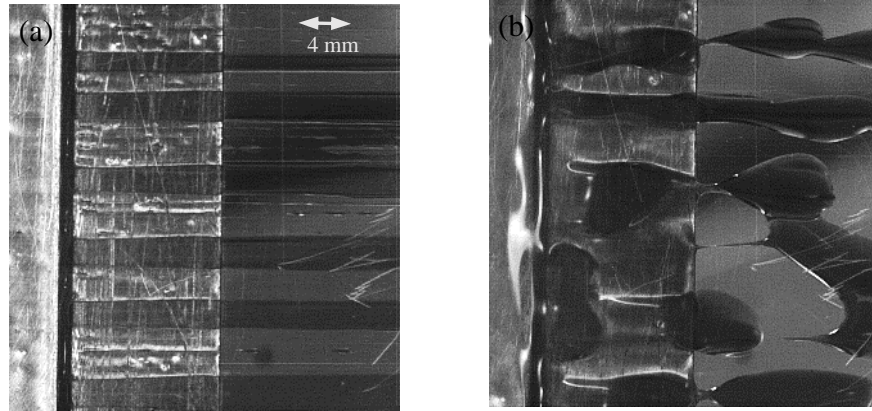
Figure 13: Images of coating defect at different coating gaps for 10 wt% fumed silica dispersion in PPG. The images include for coating gaps of a) 0.1 mm at Q = 22.2 mm^3/s, V = 10.2 mm/s, b) 0.5 mm at Q = 36.1 mm^3/s, V = 8.3 mm/s.
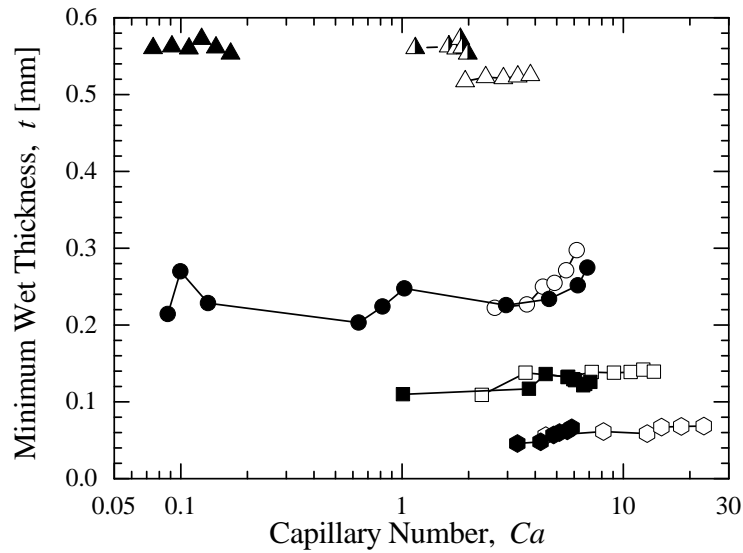

Figure 14: Minimum wet thickness, t, as a function of capillary number, Ca, for 10 wt% fumed silica dispersion in PPG (filled symbols) and silicone oil with η = 30 Pa.s (hollow symbols). The data include for different coating gaps: ($\bigcirc$) 0.1 mm, ($\blacksquare$) 0.25 mm, ($\bullet$) 0.5 mm and ($\blacktriangle$) 1 m. The capillary number is evaluated as, Ca = $\eta(\dot{\gamma})V_c/\sigma$, where the data evaluated using $\dot{\gamma} = Vc/H$ is shown in filled symbols and for data evaluated for 1 mm coating gap using $\dot{\gamma} = 6Q/(WL^2)$ is shown in shaded symbols.